Electrostatic Interactions That Determine the Rate of Pseudorotation Processes in Oxyphosphorane Intermediates: Implications with Respect to the Roles of Metal Ions in the Enzymatic Cleavage of RNA

Tadafumi Uchimaru,*[,†] Masami Uebayasi,[‡] Takuji Hirose,[†] Seiji Tsuzuki,[†] Ari Yliniemelä,[†,⊥] Kazutoshi Tanabe,[†] and Kazunari Taira[‡,∥]

National Institute of Materials and Chemical Research, National Institute of Bioscience and Human Technology, Agency of Industrial Science and Technology, MITI, and Institute of Applied Biochemistry, University of Tsukuba, Tsukuba Science City, 305 Japan

Received August 16, 1995[⊗]

The enzymatic cleavage of RNA takes place via a cyclic pentacoordinate oxyphosphorane intermediate/transition state. We carried out ab initio investigations on the neutral cyclic oxyphosphorane, which exists as a stable intermediate. As a consequence of the conformational preferences of the pentacoordinate trigonal bipyramidal intermediates, the rotation of the P−OH bonds is strongly coupled with the reaction coordinate for the pseudorotation process. In addition, the neutral PF_4OH species has a higher barrier to pseudorotation than the corresponding anionic species PF_4O^-. These findings are related to the positive charge of the hydrogen atoms on the equatorial oxygens in the trigonal bipyramidal structures: the hydrogen atoms preferably adopt eclipsed positions relative to the axial ligands. Fixing the cationic species in these regions causes an increase in the barrier heights for pseudorotation processes and, thus, prevents isomerization by pseudorotation. Consequently, metal coordination in the double-metal ion mechanism for enzymatic cleavage of RNA should serve to exclusively stabilize the trigonal bipyramidal intermediate/transition state for the in-line attack and departure process.

Introduction

The enzymatic cleavage of RNA takes place via a cyclic pentacoordinate trigonal bipyramidal oxyphosphorane intermediate/transition state (**1**).[1−4] We previously performed ab initio molecular orbital calculations on cyclic model oxyphosphoranes, considering both dianionic[5−10] and monoanionic[10,11] species (Scheme 1, species **2a** and **2b**). Lim and Karplus[12] and our group[10] reported that a potential minimum corresponding to a dianionic trigonal bipyramidal oxyphosphorane could not be located, which indicates that a dianionic intermediate does not exist in the gas phase. Protonation of one of the anionic nonbridging oxygens in the dianionic species **2a** gives rise to monoanionic species **2b**. In contrast to dianionic **2a**, the monoanionic species **2b** was found to have a well with a kinetically meaningful depth.[10,11] Moreover, we explored the reaction energy profiles for in-line attack and departure via cyclic oxyphosphoranes **2a**[7,9] and **2b**.[11] Irrespective of whether or not the pentacoordinate intermediate exists on the potential surface, the reaction energy profiles for **2a** and **2b** showed the same trend: the endocyclic P−O(2′) bond is intrinsically weaker than the exocyclic P−O(5′) bond.[7−11] The departure of exocyclic oxygen O(5′) from the oxyphosphorane species should, thus, be the rate-limiting step. This conclusion provided a qualitative interpretation of the results from mutagenesis of Barnase and RNase T_1.[8]

Scheme 1

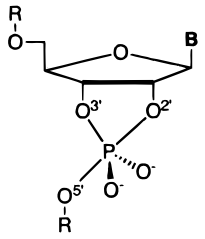

1

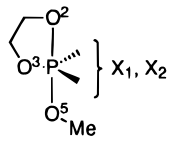

2a: $X_1 = X_2 = O^-$
2b: $X_1 = O^-$, $X_2 = OH$
2c: $X_1 = X_2 = OH$

In the catalytic active sites for enzymatic cleavage of RNA, cationic species surround the pentacoordinate oxyphosphorane intermediate;[13−16] the negative charges on the intermediate should, thus, be neutralized to a significant extent. The dianionic species **2a** was a model system representing one end-most extremity, with two negative charges associated solely with oxyphosphorane

† National Institute of Materials and Chemical Research.
‡ National Institute of Bioscience and Human Technology.
∥ Institute of Applied Biochemistry, University of Tsukuba.
⊥ On leave form Technical Research Centre of Finland, Chemical Laboratory, P.O. Box 204, SF-02151, Finland. A.Y. participated in this study as a visiting researcher at National Institute of Materials and Chemical Research.
⊗ Abstract published in *Advance ACS Abstracts,* February 1, 1996.

(1) Breslow, R.; Labelle, M. *J. Am. Chem. Soc.* **1986**, *108*, 2655−2659.
(2) Taira, K. *Bull. Chem. Soc. Jpn.* **1987**, *60*, 1903−1909.
(3) Anslyn, E.; Breslow, R. *J. Am. Chem. Soc.* **1989**, *111*, 4473−4482.
(4) Kuusela, S.; Lönnberg, H. *J. Chem. Soc. Perkin Trans. 2* **1994**, 2109−2113.
(5) Taira, K.; Uebayasi, M.; Maeda, H.; Furukawa, K. *Protein Eng.* **1990**, *3*, 691−701.
(6) Storer, J. W.; Uchimaru, T.; Tanabe, K.; Uebayasi, M.; Nishikawa, S.; Taira, K. *J. Am. Chem. Soc.* **1991**, *113*, 5216−5219.
(7) Taira, K.; Uchimaru, T.; Tanabe, K.; Uebayasi, M.; Nishikawa, S. *Nucleic Acids Res.* **1991**, *19*, 2747−2753.
(8) Uchimaru, T.; Storer, J. W.; Tanabe, K.; Uebayasi, M.; Nishikawa, S.; Taira, K. *Biochem. Biophys. Res. Commun.* **1992**, *187*, 1523−1528.
(9) Taira, K.; Uchimaru, T.; Storer, J. W.; Yliniemela, A.; Uebayasi, M.; Taira, K. *J. Org. Chem.* **1993**, *58*, 3009−3017.
(10) Uebayasi, M.; Uchimaru, T.; Koguma, T.; Sawata, S.; Shimayama, T.; Taira, K. *J. Org. Chem.* **1994**, *59*, 7414−7420.
(11) Uebayasi, M.; Uchimaru, T.; Taira, K. *Chem. Express* **1992**, *7*, 617−620.
(12) Lim, C.; Karplus, M. *J. Am. Chem. Soc.* **1991**, *112*, 5872−5873.
(13) Beese, L. S.; Steitz, T. A. *EMBO J.* **1991**, *10*, 25−33.
(14) Yarus, M. *FASEB J.* **1993**, *7*, 31−39.
(15) Steitz, T. A.; Steitz, J. A. *Proc. Natl. Acad. Sci. U.S.A.* **1993**, *90*, 6498−6502.
(16) Pyle, A. M. *Science* **1993**, *261*, 709−714.

0022-3263/96/1961-1599$12.00/0

Table 1. RHF and MP2 Energies of the Stationary Points of 2c and 2b

structure	RHF/6-31+G*//RHF/6-31+G* energy[a]	relative energy[b]	RMP2/6-31+G*//RHF/6-31+G* energy[a]	relative energy[b]	ZPE[c]	imaginary frequency[d]
			Neutral Species **2c**			
$I^{ee}1$	833.954 35	0.0	835.371 15	0.0	96.47	–
$I^{ee}2$	833.951 92	1.5	835.369 05	1.3	96.42	–
$I^{ee}3$	833.950 97	2.1	835.367 88	2.1	96.48	–
$I^{ee}4$	833.950 77	2.2	835.367 78	2.1	96.49	–
$I^{ae}5$	833.951 42	1.8	835.368 14	1.9	96.11	–
$I^{ae}6$	833.947 69	4.2	835.365 19	3.7	96.13	–
TS_{en}	833.910 23	27.7	835.335 13	22.6	92.18	1429.8*i*
TS_{ex}	833.896 75	36.1	835.328 52	26.8	92.76	1923.7*i*
$TS_{rot.}1$	833.942 53	7.4	835.360 43	6.7	95.57	378.1*i*
$TS_{rot.}2$	833.936 59	11.1	835.354 99	10.1	95.32	377.3*i*
$TS_{pr}1$	833.942 40	7.5	835.361 08	6.3	95.89	99.9*i*
$TS_{pr}2$	833.937 66	10.5	835.356 55	9.2	95.66	192.6*i*
			Monoanionic Species **2b**			
$I^{e}1$	833.390 90	0.0	834.828 80	0.0	87.06	–
$I^{e}2$	833.391 11	0.1	834.828 86	0.0	87.01	–
$I^{a}5$	833.378 24	7.9	834.816 70	7.6	86.41	–
$I^{a}6$	833.380 91	6.3	834.819 80	5.6	86.59	–
$TS_{pr}2'$	833.378 98	7.5	834.817 70	7.0	86.43	81.8*i*

[a] Absolute energies in -au. [b] Relative energies in kcal/mol. [c] Zero point energies in kcal/mol, calculated at the HF level (not scaled). [d] Wave number of imaginary frequencies in cm^{-1}, calculated at the HF level.

itself, and no interaction existing between anionic oxyphosphorane and cationic species. We now consider in detail the fully protonated species **2c**, the other end-most model, in which the negative charges are completely neutralized. In addition, the values of the first and second pK_a were estimated to be around 9 and 13, respectively,[17] which suggests that the oxyphosphorane intermediate should exist mainly as the neutral species **2c** in aqueous solutions, with the exception of highly basic media. We have, therefore, carried out ab initio investigations on **2c**. We have compared the electronic properties of neutral **2c** with those of dianionic and monoanionic **2a** and **2b**, respectively. In addition, the reaction coordinates for the exchange of ligand positions in the trigonal bipyramidal structures have been explored (Berry pseudorotation: Figure 1). We describe here our speculations on the roles of neutral species and of the coordination of metal ions in the enzymatic cleavage of RNA.

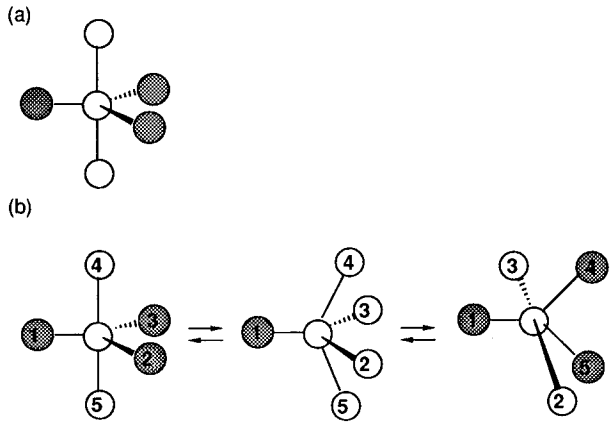

Figure 1. (a) Schematic representation of the structure of pentacoordinate trigonal bipyramidal species. The trigonal bipyramidal species has two types of ligand: equatorial ligands (filled circles) and axial ligands (open circles). (b) The trigonal bipyramidal species undergoes an exchange of ligand positions via a square pyramidal structure (a Berry pseudorotation mechanism). Two equatorial ligands move to the axial positions, and two axial ligands move to the equatorial positions. The pivot atom remains in the equatorial position, and it occupies the apical position in the square pyramidal transition state (the atom numbered 1).

Details of Computations

We performed ab initio calculations using the Gaussian 92 program.[18] Streitwieser *et al.* suggested that d-functions, in particular on phosphorus, were necessary for effective polarization stabilization of the anionic charge in their analysis of hypervalent phosphorus compounds.[19] Incorporation of diffuse functions was essential for representation of the electronic structures of anionic species.[20,21] To evaluate the difference between neutral and anionic species, we utilized the 6-31+G* basis set. We optimized the geometries at the Hartree–Fock (HF) level and then performed the vibrational frequency calculations for each stationary point. Energies of each stationary point were evaluated by MP2 (frozen core) single-point calculations. We estimated the net charges of the atoms using the generalized second-order densities.[22] In addition, we carried out NBO analyses[23–27] to examine hyperconjugative interactions. The points that yielded the energy profiles shown in

(17) Kluger, R.; Covitz, F.; Dennis, E.; Williams, L. D.; Westheimer, F. H. *J. Am. Chem. Soc.* **1969**, *91*, 6066–6072.
(18) Frish, M. J; Trucks, G. W.; Head-Gordon, M.; Gill, P. M. W.; Wong, M. W.; Foresman, J. B.; Johnson, B. G.; Schlegel, H. B.; Robb, M. A.; Replogle, E. S.; Gomperts, R.; Anfres, J. L.; Raghavachari, K.; Binkley, J. S.; Gonzalez, C.; Martin, D. J.; Fox, D. J.; Defrees, D. J.; Baker, J.; Stewart, J. J. P.; Pople, J. A. Gaussian, Inc., Pittsburgh PA, **1992**.
(19) Streitwieser, A., Jr.; Rajca, A.; McDowell, R. S.; Glaser, R. *J. Am. Chem. Soc.* **1987**, *109*, 4184–4188.
(20) Clark, T.; Chandrashekhar, J.; Spitznagel, G. W.; Schleyer, P. v. R. *J. Comput. Chem.* **1983**, *4*, 294–301.
(21) Spitznagel, G. W.; Clark, T.; Schleyer, P. v. R.; Hehre, W. J. *J. Comput. Chem.* **1987**, *8*, 1109–1116.
(22) Handy, N. C.; Schaefer, H. F., III. *J. Chem. Phys.* **1984**, *81*, 5031–5033.
(23) Foster, J. P.; Weinhold, F. *J. Am. Chem. Soc.* **1980**, *102*, 7211–7218.
(24) Reed, A. E.; Weinhold, F. *J. Chem. Phys.* **1983**, *78*, 4066–4073.
(25) Reed, A. E.; Weinstock, R. B.; Weinhold, F. *J. Chem. Phys.* **1985**, *83*, 735–746.
(26) Carpenter, J. E.; Weinhold, F. *THEOCHEM* **1988**, *169*, 41–62.
(27) Reed, A. E.; Curtiss, L. A.; Weinhold, F. *Chem. Rev.* **1988**, *88*, 899–926.

Table 2. RHF and MP2 Energies of the Stationary Points of PF_4OH and PF_4O^-

structure	symmetry	RHF/6-31+G*//RHF/6-31+G* energy[a]	RHF/6-31+G*//RHF/6-31+G* relative energy[b]	RMP2/6-31+G*//RHF/6-31+G* energy[a]	RMP2/6-31+G*//RHF/6-31+G* relative energy[b]	ZPE[c]	imaginary frequency[d]
			PF_4OH				
TBP[e]	C_s	814.072 96	0.0	815.075 89	0.0	19.84	–
TBP[a]	C_s	814.055 03	11.3	815.059 08	10.5	19.19	–
$TS^e_{rot.}$	C_s	814.055 98	10.7	815.058 61	10.8	18.40	551.1*i*
$TS^a_{rot.}$	C_s	814.053 20	12.4	815.057 61	11.5	18.81	260.0*i*
$TS_{pr}1$	C_s	814.057 24	9.9	815.061 56	9.0	18.76	247.0*i*
$TS_{pr}1'$	C_s	814.055 54	10.9	815.059 04	10.6	18.38	99.2*i*[e]
$TS_{pr}2$	C_1	814.054 76	11.4	815.059 49	10.3	19.28	83.5*i*
$TS_{pr}2'$	C_1	814.052 90	12.6	815.057 85	11.3	18.94	153.3*i*
			PF_4O^-				
TBP[e]	C_{2v}	813.554 11	0.0	814.575 53	0.0	10.95	–
TBP[a]	C_{3v}	813.515 05	24.5	814.541 22	21.5	10.58	–
$TS_{pr}1$	C_{4v}	813.549 14	3.1	814.571 85	2.3	10.79	124.2*i*

[a] Absolute energies in -au. [b] Relative energies in kcal/mol. [c] Zero point energies in kcal/mol, calculated at the HF level (not scaled). [d] Wave number of imaginary frequencies in cm^{-1}, calculated at the HF level. [e] A second-order transition state. The imaginary frequency along the reaction coordinate for pseudorotation is given.

Figures 3, 4, 6, and 7 were obtained through geometry optimizations at each value of the reaction coordinate without any additional constraints. The graphic representation of electrostatic potentials (Figure 9) was generated with the SPARTAN program package.[28]

Nomenclature. We identify structures in the following manner. "**I**" represents the local minima of either neutral **2c** or monoanionic **2b**. The subscripts "en" and "ex" following "**TS**" indicate transition states for cleavage/formation of endocyclic and of exocyclic bonds, respectively. The local minima of PF_4OH and PF_4O^- are represented by "**TBP**" (trigonal bipyramid). The superscripts "a" and "e" are positional identifiers indicating whether hydroxyl substituents (oxy anion in the case of PF_4O^-) occupy an axial or an equatorial position. The subscripts "rot" and "pr" following "**TS**" allow us to distinguish between rotational and pseudorotational transition states.

Results

Pentacoordinate Intermediates for the Neutral and Monoanionic Species 2c and 2b. According to Westheimer's guidelines,[29,30] nucleophilic attack of the 2′ oxygen atom on phosphorus results in an oxyphosphorane intermediate with O(2′) and O(5′) oxygen ligands at axial positions. We found that neutral oxyphosphorane **2c** had four such trigonal bipyramidal structures $\mathbf{I^{ee}1}$ through $\mathbf{I^{ee}4}$. In addition to these structures, we found the stable conformers $\mathbf{I^{ae}5}$ and $\mathbf{I^{ae}6}$ (Figure 2).

Karplus's group[31] and our own group[32] concluded previously that the rotation of the equatorial P−OMe bond in the trimethoxyphosphorane system was essential for the lowest-energy pathway for the base-catalyzed methanolysis and hydrolysis of dimethyl phosphate. Similar bond rotation was observed in the studies on the reaction profiles for in-line attack and departure processes via the monoanionic oxyphosphorane **2b**[11] and the related monoanionic phosphoranes.[33−35] We were able to locate the transition states $\mathbf{TS_{rot.}1}$ and $\mathbf{TS_{rot.}2}$ for such rotation of equatorial O−H bond in **2c** (Figure 2). The most stable intermediate $\mathbf{I^{ee}1}$ leads to $\mathbf{I^{ee}4}$ via these transition states by rotating the equatorial P−OH bond. The MP2 energy evaluations suggested barrier heights of 6.7 and 10.1 kcal/mol for these bond rotations.

We also optimized several conformers of monoanionic oxyphosphorane **2b**. Removal of one of the hydrogens on the equatorial hydroxyl groups of neutral minima $\mathbf{I^{ee}1}$ and $\mathbf{I^{ee}4}$ resulted in the monoanionic minimum $\mathbf{I^e1}$. Neutral minima $\mathbf{I^{ee}2}$ and $\mathbf{I^{ee}3}$ gave another monoanionic minimum $\mathbf{I^e2}$. Removal of the same proton from $\mathbf{I^{ae}5}$ and $\mathbf{I^{ae}6}$ yielded the monoanionic minima $\mathbf{I^a5}$ and $\mathbf{I^a6}$, with axial hydroxyl groups (Figure 2).

Reaction Profile for In-Line Attack and Departure Process via Neutral 2c. Starting from the most stable neutral trigonal bipyramidal minimum $\mathbf{I^{ee}1}$, we explored the reaction energy profiles for the in-line attack and departure process (Figure 3). We located the transition states for cleavage/formation of the axial endocyclic P−O(2′) bond and of the exocyclic P−O(5′) bond ($\mathbf{TS_{en}}$ and $\mathbf{TS_{ex}}$).

The transition states $\mathbf{TS_{en}}$ and $\mathbf{TS_{ex}}$ clearly involve processes of intramolecular proton migration. The major components of the eigenvectors corresponding to the imaginary frequencies for these transition states indicated the migration of hydrogen atoms between the nonbridging oxygen and the attacking/departing oxygen. The generalized second-order densities suggested net charges of +0.62e and +0.60e, respectively, for the migrating hydrogen atoms in the transition states $\mathbf{TS_{en}}$ and $\mathbf{TS_{ex}}$. In the minimum structures $\mathbf{I^{ee}1}$ through $\mathbf{I^{ee}4}$, the hydrogen atoms on the nonbridging P−O bonds are located in roughly eclipsed positions relative to the axial P−O bonds. The torsion angles about $H-O-P-O_{ax}$ are close to 0° or 180°. The torsion angles remain almost unchanged in the transition states $\mathbf{TS_{en}}$ and $\mathbf{TS_{ex}}$. In the transition states, one of the hydrogen atoms on the nonbridging equatorial oxygens is located between the original oxygen and the attacking/departing axial oxygen.[36] Proximity between the positively charged hydrogen atom and the attacking/departing oxygen results in favorable electrostatic interactions that stabilize the transition states.

The proton migration promotes development of a negative charge on the nonbridging oxygen and neutral-

(28) Carpenter, J. E.; Hehre, W. J.; Kahn, S. D. SPARTAN version 3.0 Wavefunction Inc., 18401 Von Karmen, #370 Irvine, CA 92715.
(29) Westheimer, F. H. *Acc. Chem. Res.* **1968**, *1*, 70−78.
(30) Thatcher, G. R. J.; Kluger, R. *Adv. Phys. Org. Chem.* **1989**, *25*, 99−265.
(31) Dejaegere, A.; Lim, C.; Karplus, M. *J. Am. Chem. Soc.* **1991**, *113*, 4353−4355.
(32) Uchimaru, T.; Tanabe, K.; Nishikawa, S.; Taira, K. *J. Am. Chem. Soc.* **1991**, *113*, 4351−4353.
(33) Lim, C.; Tole, P. *J. Phys. Chem.* **1992**, *96*, 5217−5219.
(34) Tole, P.; Lim, C. *J. Phys. Chem.* **1993**, *97*, 6212−6219.
(35) Tole, P.; Lim, C. *J. Am. Chem. Soc.* **1994**, *116*, 3922−3931.

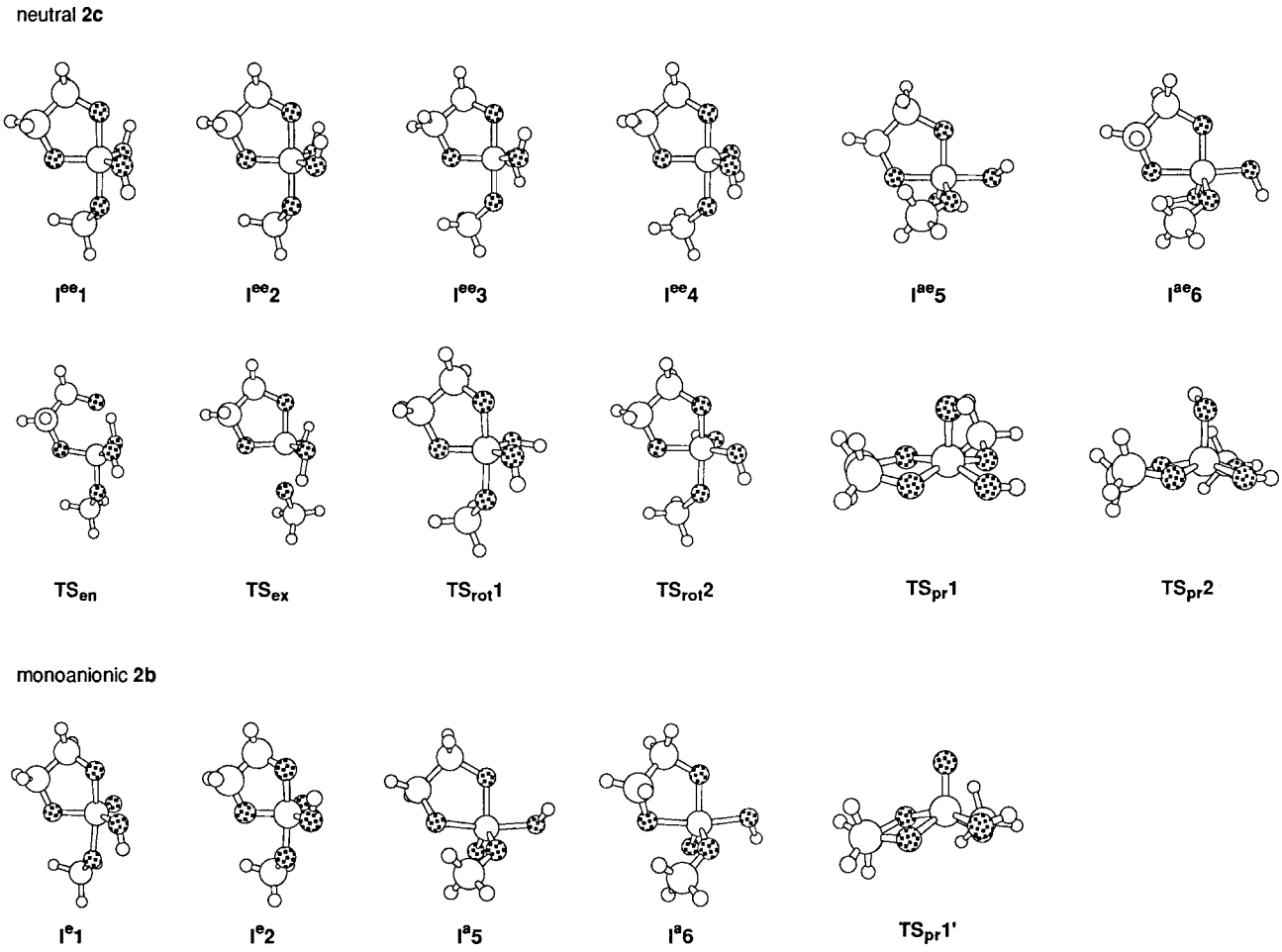

Figure 2. Optimized geometries of neutral and monoanionic oxyphosphoranes **2c** and **2b**.

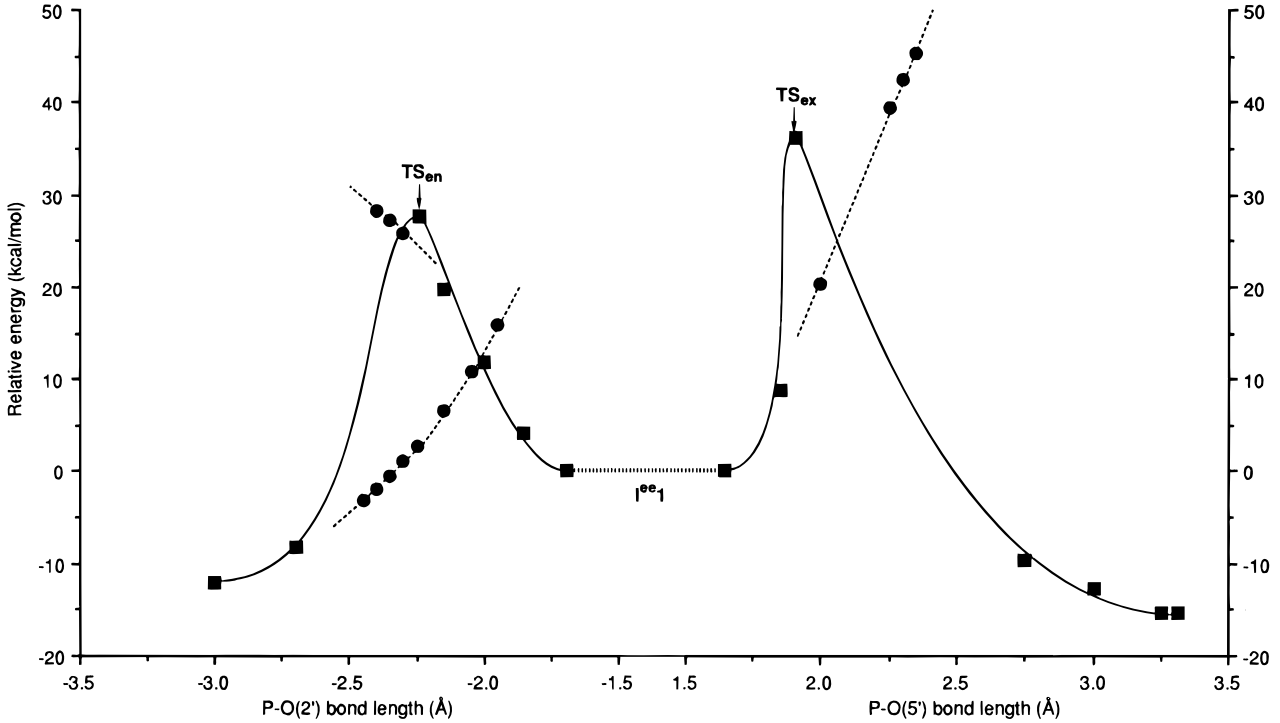

Figure 3. Energy profile for the in-line attack and departure process via the most stable pentacoordinate intermediate (**I^{ee}1**) for neutral species **2c**. The P−O(2′) and P−O(5′) bond distances were used as reaction coordinates. The vertical axis shows the energy in kcal/mol relative to **I^{ee}1**. Broken lines connecting filled circles represent the energy profiles without the migration of protons (see text).

izes the incipient negative charge on the departing oxygen. Unless the proton migration took place, a neutral oxyphosphorane species encountered a significantly high barrier for expulsion of its axial ligand (see broken lines in Figure 3). Thus, the charge redistribution of the neutral oxyphosphorane must be allowed for the

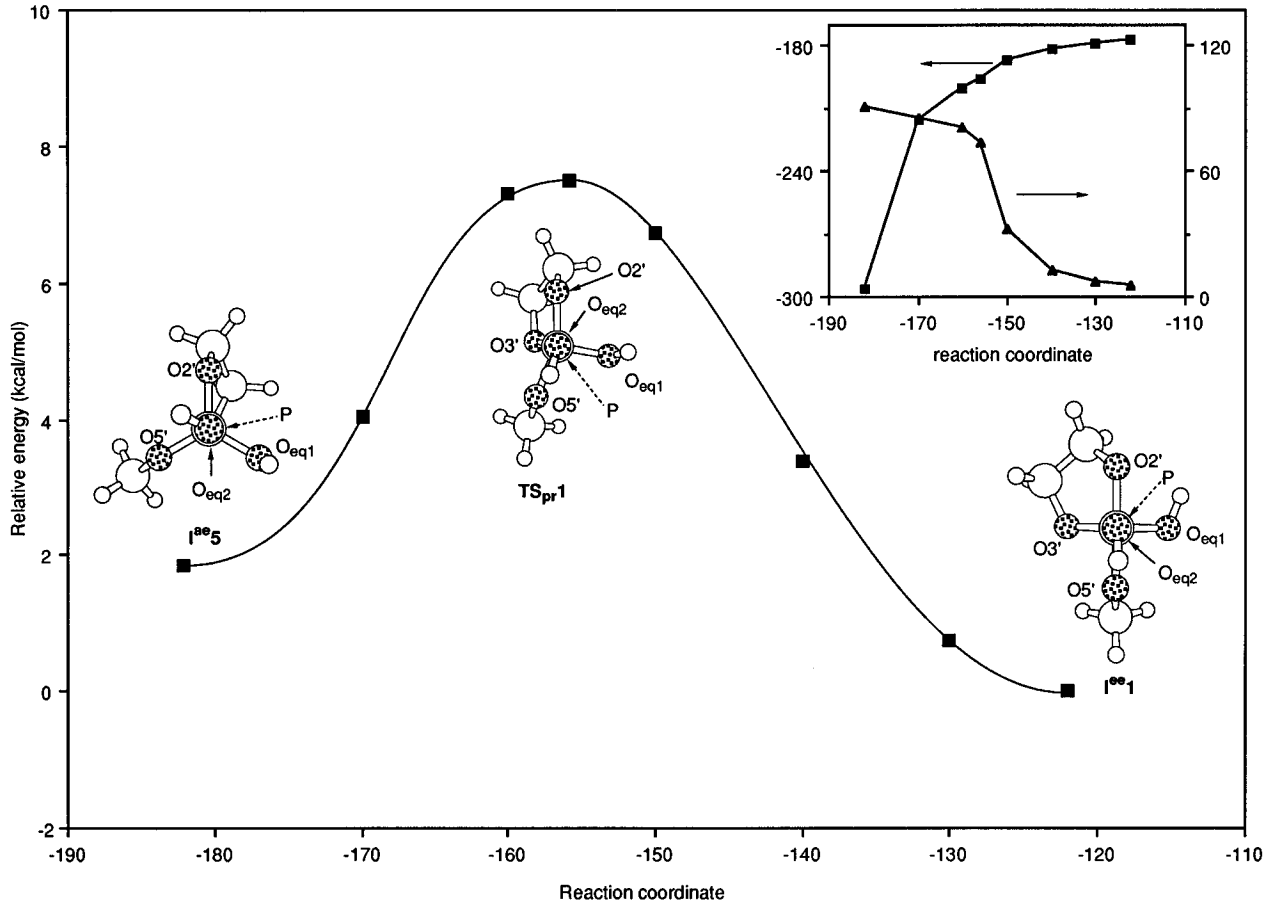

Figure 4. Energy profile for the pseudorotation process that leads the most stable trigonal bipyramidal minimum **I^{ee}1** to the end product **I^{ae}5** via the transition state **TS$_{pr}$1**. The torsion angle about O_{eq2}-P−O2′-O3′ was used as the reaction coordinate. The hydrogen on O_{eq1} occupies an eclipsed position relative to the axial P−O(2′) bond in the initial structure of **I^{ee}1**. The P−O_{eq1} bond rotates toward the equatorial O_{eq2} during the pseudorotation. The hydrogen on O_{eq1} eventually adopts the eclipsed position relative to O_{eq2} which occupies, finally, the axial position in the end product of the pseudorotation. Meanwhile, the O_{eq2}−H bond lies parallel to the axial P−O(2′) and P−O(5′) bonds in **I^{ee}1**. The P−O_{eq2} bond also rotates during the pseudorotation process. The hydrogen on O_{eq2} is ultimately located between the O(2′) and O(5′) atoms which both occupy equatorial positions after pseudorotation. Inset: the changes of the torsion angle about H−O_{eq1}−P−O2′ (filled triangles) and H−O_{eq2}−P−O2′ (filled squares) during the pseudorotation process.

formation/cleavage of the axial P−O bond. A similar trend was observed for the reaction profile via the partially protonated monoanionic oxyphosphorane **2b**.[11] The monoanionic and neutral oxyphosphorane species **2b** and **2c** stand in striking contrast to the dianionic species **2a**, which has no pentacoordinate intermediate in the gas phase. Thus, we can safely conclude that the depth of the well for the oxyphosphorane intermediate is critically dependent on its protonation state. The neutralization of the phosphate oxy anion significantly increases its stability.

Pseudorotation Processes for the Cyclic Neutral and Monoanionic Species 2c and 2b. The neutral and monoanionic species **2c** and **2b** were shown to have several trigonal bipyramidal minima, in which ligand positions have been exchanged. The pseudorotation processes should, thus, connect these minima. If the ring oxygen were to act as a pivot atom in a pseudorotation process, the neutral and monoanionic oxyphosphoranes **2c** and **2b** would yield a diequatorial ring. Diequatorial ring structure is highly strained and considerably unstable.[29,30,37] Consequently, the pseudorotation processes with hydroxyl oxygen acting as the pivot atom are the most likely for the neutral and the monoanionic oxyphosphoranes **2c** and **2b**.

We located the pseudorotational transition states **TS$_{pr}$1** and **TS$_{pr}$2** for neutral species **2c**. The pentacoordinate structures **I^{ee}1** and **I^{ee}4** pseudorotate to give structures **I^{ae}5** and **I^{ae}6**, respectively, via these square pyramidal transition states. The end products **I^{ae}5** and **I^{ae}6** were found to be only 1.9 and 3.7 kcal/mol higher in MP2 energy than the most stable minimum **I^{ee}1**. The energy evaluations at the MP2 level suggested activation barriers of about 6 or 7 kcal/mol for these pseudorotations. For monoanionic species, we were able to locate the pseudorotational transition state **TS$_{pr}$2′**. This transition state, which corresponds to the neutral transition state **TS$_{pr}$2**,[38] connects the monoanionic intermediates **I^{e}1** and **I^{a}6**. The MP2 energy of **TS$_{pr}$2′** is 7.0 kcal/mol higher than that of **I^{e}1**.

The hydrogen atoms on the equatorial P−O bond occupy eclipsed positions relative to the axial P−O bonds in the trigonal bipyramidal intermediates. Meanwhile, the hydrogens on the axial P−O bond are located in gauche positions relative to the equatorial ligands. The neutral and monoanionic intermediates **2c** and **2b** both

(36) The distance between the hydrogen atom and the departing oxygen is reduced from 2.132 to 1.319 Å when **I^{ee}1** is converted to the endocyclic transition state **TS$_{en}$**. Conversely, the distance between the hydrogen and the original oxygen is increased from 0.948 to 1.108 Å. For the exocyclic transition state **TS$_{ex}$**, the corresponding distances vary from 2.058 to 1.187 Å and from 0.950 to 1.232 Å, respectively.

(37) Holmes, R. R. *J. Am. Chem. Soc.* **1978**, *100*, 433−446.

(38) We were unable to locate the monoanionic saddle point corresponding to the neutral transition state **TS$_{pr}$1**.

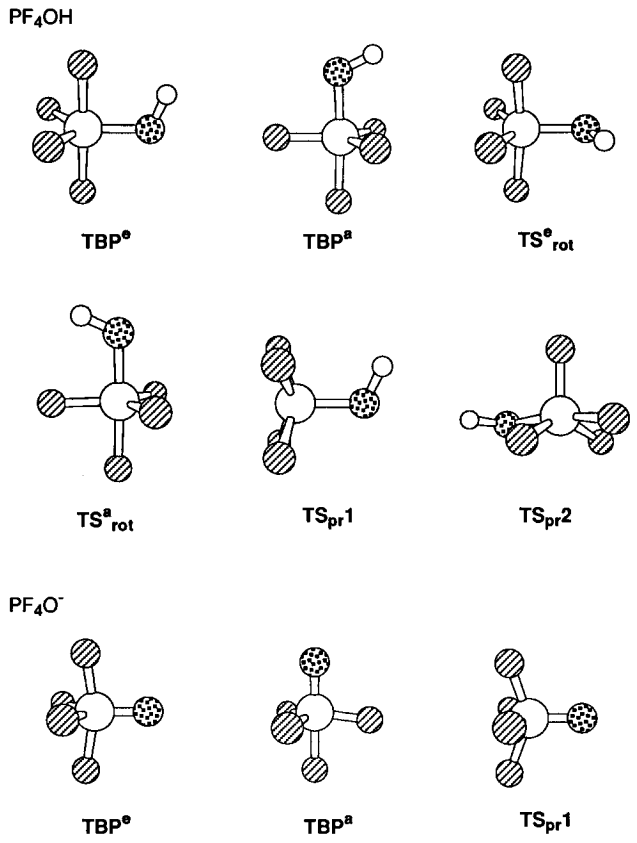

Figure 5. Optimized geometries of PF_4OH and PF_4O^-.

show these conformational preferences. As a consequence of these conformational preferences, the rotation of the P−OH bond is strongly coupled with the reaction coordinates of the pseudorotation processes of **2c** (Figure 4). The structure of the monoanionic transition state **TS$_{pr}$2′** also suggests the rotation of the P−OH bond during the exchange of ligand positions.

As we discuss in the following sections, the conformational preferences of P−OH bonds are derived from hyperconjugative and electrostatic interactions. Trigonal bipyramidal oxyphosphoranes always involve such interactions. Thus, this type of conformational change of the P−OH bond will occur during any other pseudorotation processes that are possible for neutral **2c**, as well as for monoanionic **2b**.[39]

Pseudorotation Processes for PF_4OH. In an attempt to generalize the features of pseudorotation processes, we carried out further investigations on the simplified system, PF_4OH. The conformational preferences for the P−OH bond in PF_4OH are similar to those discussed for cyclic oxyphosphoranes **2c** and **2b**. The O−H bond is eclipsed by the axial P-F bond in the global minimum **TBP^e**, while the axial O−H bond occupies a staggered position in the second minimum **TBP^a** (Figure 5). Rotation of the equatorial P−OH bond in **TBP^e** by 90° yielded another C_s structure, namely a rotational transition state for the equatorial P−OH bond (**TS$^e_{rot.}$**). The rotational transition state for the axial P−OH bond also has C_s symmetry (**TS$^a_{rot.}$**). The axial OH group occupies an eclipsed position relative to the equatorial fluorine atom in **TS$^a_{rot.}$**.

The rotation of the P−OH bond is also strongly coupled with the reaction coordinates for the pseudorotation processes for PF_4OH. Figure 6 shows the energy profile for the pseudorotation that connects two global minimum structures **TBP^e** via a square pyramidal transition state, **TS$_{pr}$1**. A hydroxyl oxygen acts as the pivot in this pseudorotation process. In the other pseudorotation process that connects the global minimum and the second minimum (**TBP^e** and **TBP^a**), one of the equatorial fluorine atoms acts as the pivot atom (Figure 7). The

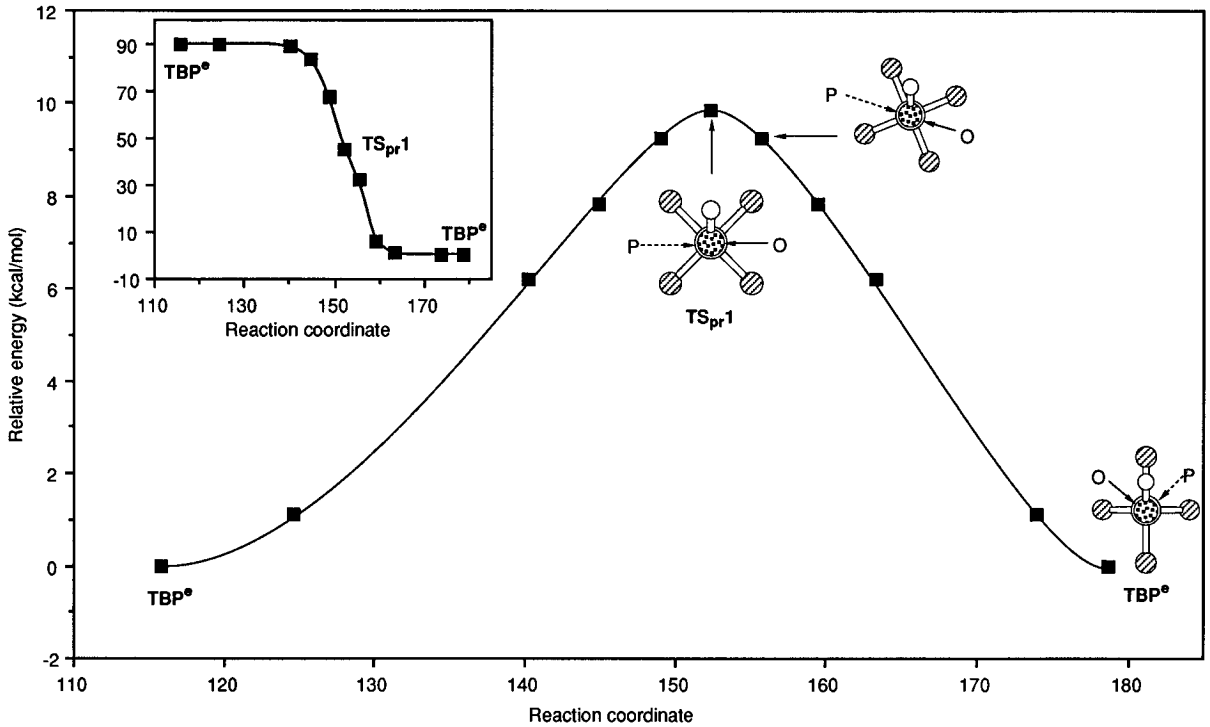

Figure 6. Energy profile for the pseudorotation of PF_4OH that connects two identical **TBP^e** structures. The angle about $F_{ax(eq)}$−P−$F_{ax(eq)}$ was used as the reaction coordinate. The vertical axis shows the energy in kcal/mol relative to the structure of **TBP^e**. Since the structures at both ends are exactly the same, the energy profile is symmetric. Correspondingly, the transition-state structure has *Cs* symmetry, and the pivot oxygen atom occupies the apical position in the square pyramidal structure. The OH bond, which is eclipsed by the axial fluorine atom in both end structures (**TBP^e**), is staggered relative to the basal fluorine ligands in the transition state. Inset: the changes in the torsion angle about H−O−P−F during the pseudorotation process.

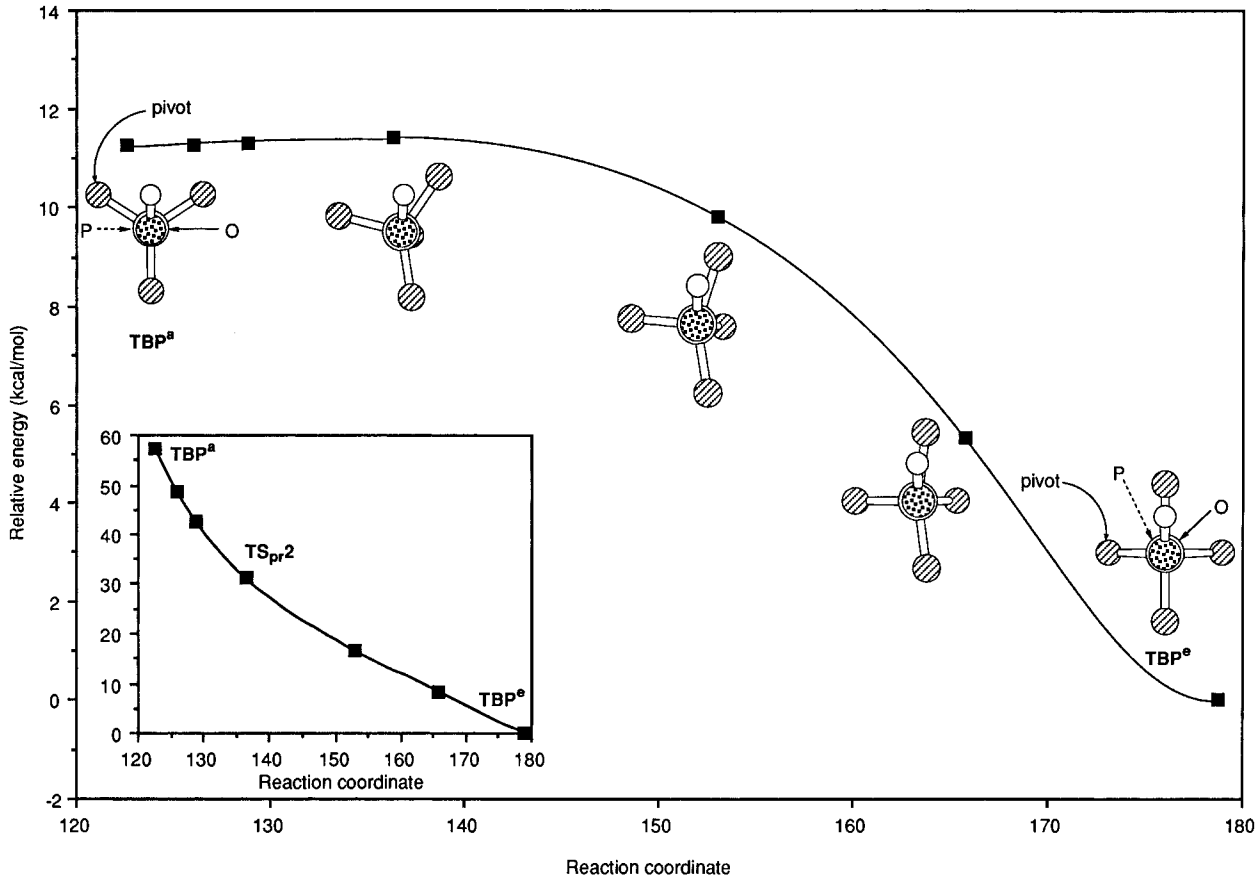

Figure 7. Energy profile for the pseudorotation process of PF_4OH that connects the **TBP^e** and **TBP^a** structures. The bond angle about $F_{ax}-P-F_{ax}$ in the **TBP^e** structure was used as the reaction coordinate. The OH bond lies parallel to the axial P−F bond in the **TBP^e**. The P−OH bond rotates toward the pivot fluorine atom during the pseudorotation. Finally, the proton is located between two fluorine atoms in the end product, **TBP^a**, of this pseudorotation. Inset: the changes in the torsion angle about H−O−P−F during the pseudorotation process.

second minimum, **TBP^a**, is 11.3 kcal/mol higher in HF absolute energy than the global minimum **TBP^e**. The transition-state structure **TS$_{pr}$2** for this pseudorotation closely resembles that of the second minimum **TBP^a**, in accord with Hammond postulate.[43]

Fixing the conformation of the P−OH bond increased, not unexpectedly, the barrier heights for pseudorotation processes. However, the increases in barrier heights were not significant. If the C_s plane in the **TBP^e** structure is maintained in the pseudorotation process shown in Figure 6, the initial **TBP^e** structure should lead to the rotational transition state **TS$^e_{rot.}$**, via the second-order transition state **TS$_{pr}$1′**. In this putative process, the torsion angle about H-O-P-F is kept at 0° all along the reaction coordinate. The HF absolute energy of the putative **TS$_{pr}$1′** is only 1.0 kcal/mol higher than that of transition state **TS$_{pr}$1** in Figure 6. We also considered a putative process for the other pseudorotation that connects structures **TBP^e** and **TBP^a** (Figure 7). The torsion angle about $H-O-P-F_{ax}$ in **TBP^e** is 0°. If this torsion angle is maintained, the maximum energy point for the putative process corresponds to **TS$_{pr}$2′**. This putative transition state, **TS$_{pr}$2′**, connects the global minimum **TBP^e** and the rotational transition state **TS$^a_{rot.}$**. The difference in the HF absolute energy between the putative **TS$_{pr}$2′** and the transition state **TS$_{pr}$2** in Figure 7 is 1.2 kcal/mol.

Origin of Conformational Preferences of the P−OH Bond. Hyperconjugative Interactions. The conformational preference of equatorially substituted hydroxyl group clearly stems from the hyperconjugation. There are two stationary points for the equatorially hydroxyl-substituted trigonal bipyramidal structure: the global minimum **TBP^e** and the rotational transition state **TS$^e_{rot.}$**. The oxygen atom has π-type and σ-type lone pair orbitals. The former gives larger and more dominant hyperconjugative interactions than the latter.[44,45] The π-type lone pair orbital on the equatorial oxygen gives significantly larger stabilization through hyperconjugation in **TBP^e** than in **TS$^e_{rot.}$**. The structure of **TBP^e** gives a value of 14.72 kcal/mol for the second-order perturbation energy of hyperconjugation between the π-type lone pair orbital on the equatorial oxygen and the antibonding orbital of each equatorial P-F bond (Figure 8a). For the rotational transition state **TS$^e_{rot.}$**, the π-type lone pair orbital interacts with the antibonding orbital of each axial P-F bond with the significantly smaller perturbation energy of only 8.33 kcal/mol (Figure 8b). We[46] and others[47,48] reported similar trends for hyperconjugation in the related pentacoordinate phosphorane species.

(39) Cramer *et al.* have reported this type of conformational change of the P−O bond in phosphoranyl radicals during pseudoinversion, pseudorotation, and double pseudorotation processes.[40−42]

(40) Cramer, J. C. *J. Am. Chem. Soc.* **1990**, *112*, 7965−7972.

(41) Cramer, J. C.; Gustafson, S. M. *J. Am. Chem. Soc.* **1994**, *116*, 723−734.

(42) Gustafson, S. M.; Cramer, J. C. *J. Phys. Chem.* **1995**, *99*, 2267−2277.

(43) Hammond, G. S. *J. Am. Chem. Soc.* **1955**, *77*, 334−338.

(44) Reed, A. E; Schleyer, P. v. R. *Inorg. Chem.* **1988**, *27*, 3969−3987.

(45) Salzner, U.; Schleyer, P. v. R. *J. Am. Chem. Soc.* **1993**, *115*, 10231−10236.

(46) Uchimaru, T.; Tsuzuki, S.; Storer, J. W.; Tanabe, K.; Taira, K. *J. Org. Chem.* **1994**, *59*, 1835−1843.

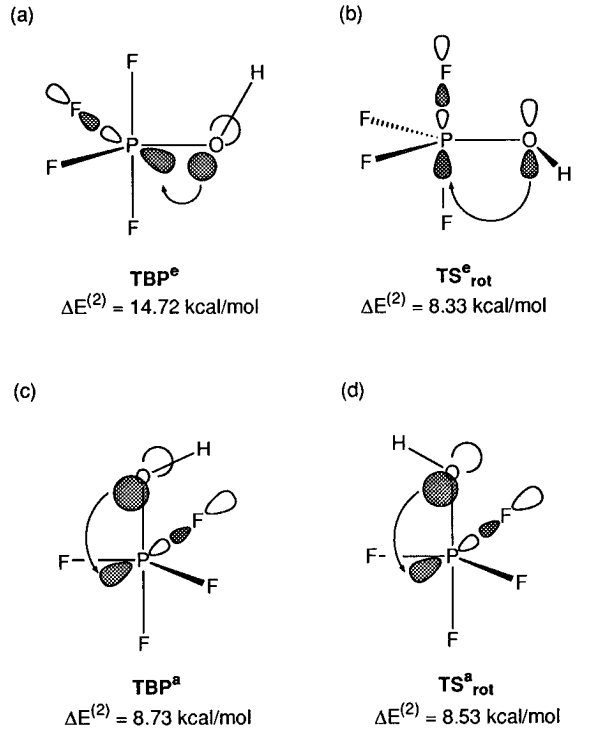

Figure 8. Hyperconjugative interactions of the π-type lone pair orbital on the oxygen atom in neutral PF_4OH. The second-order perturbation energies (ΔE^2) are given for each hyperconjugation.

The axially substituted structures **TBP**^{a} and **TS**$^a_{rot.}$ have a much smaller difference in HF absolute energy, namely 1.1 kcal/mol, than the equatorially substituted structures **TBP**^{e} and **TS**$^e_{rot.}$ (10.7 kcal/mol). Correspondingly, the hyperconjugation of the lone pair orbitals on the axial oxygen is much less sensitive to the conformation of the P−OH bond as compared to that of the lone pairs on the equatorial oxygen. The hyperconjugation between the π-type lone pair on the axial oxygen and each gauche P−F bond yields perturbation energies of 8.73 and 8.53 kcal/mol, respectively, for **TBP**^{a} and **TS**$^a_{rot.}$ (Figure 8, parts c and d).

Electrostatic Interactions. As discussed above, the transition-state structures **TS**$_{en}$ and **TS**$_{ex}$ for cleavage/formation of axial P−O(2′) and P−O(5′) bonds in neutral **2c** reveal the importance of electrostatic interactions. For the hydrogen in PF_4OH, the generalized second-order densities suggested a net charge of between +0.54e and +0.57e. A positively charged hydrogen atom should cause a favorable electrostatic interaction. The electrostatic interaction, as well as the hyperconjugative interaction, rationalized the preferred positions of hydrogen in the P−OH bond.

Removal of the proton from the PF_4OH molecule yields the monoanionic species PF_4O^-. As for the parent neutral PF_4OH, monoanionic PF_4O^- has two trigonal bipyramidal minima (**TBP**^{e} and **TBP**^{a}) and a square pyramidal pseudorotational transition state (**TS**$_{pr}$**1**) (Figure 5). We calculated the electrostatic potential for each structure. The global minimum structure **TBP**^{e} of PF_4O^-, with an oxy anion in the equatorial position, has the lowest electrostatic potential in the regions between the equatorial oxy anion and the axial fluorine atom

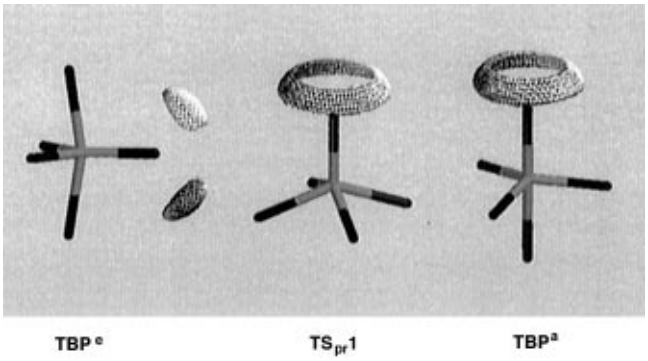

Figure 9. Electrostatic isopotential surfaces for PF_4O^- species. The electrostatic potential was calculated for the 6-31+G* optimized geometries using 6-31+G* wave functions. The values of the electrostatic potential on the surface and the lowest values of the electrostatic potential are as follows (kcal/mol): [left] **TBP**^{e} structure, −165.0, −171; [center] **TS**$_{pr}$**1** structure, −165.0, −166; [right] **TBP**^{a} structure −177.0, −178.

(Figure 9, left). Meanwhile, the regions of lowest electrostatic potential for the other minimum (**TBP**^{a}) and for the square pyramidal structure (**TS**$_{pr}$**1**) are located around the oxy anion and the potentials are less directional for both structures (Figure 9, right and center).

Two stationary points (**TBP**^{e} and **TS**$^e_{rot.}$) for equatorially hydroxyl-substituted PF_4OH have a large difference in energy (10.7 kcal/mol in HF absolute energy). This result is in accord with the directional electrostatic potential for the **TBP**^{e} structure of PF_4O^-. The preferred position of the hydrogen atom in the **TBP**^{e} structure of neutral PF_4OH is in agreement with the regions of lowest electrostatic potential. By contrast, the less directional electrostatic potential for the **TBP**^{a} structure corresponds to the small difference in energy between the two axially hydroxyl-substituted structures of PF_4OH (**TBP**^{a} and **TS**$^a_{rot.}$; 1.1 kcal/mol in HF absolute energy). In addition, fixing the conformation of the P−OH bond results in only a slight increase in the pseudorotational barrier for PF_4OH, as is readily understandable in view of the nondirectional electrostatic potential for the square pyramidal structure of PF_4O^- (**TS**$_{pr}$**1**).

The electrostatic potential for PF_4O^- is closely related to the hyperconjugation. The oxygen lone pair electrons in the equatorial plane are strongly delocalized into the equatorial P−F bonds through hyperconjugation. The lone pair orbital in the equatorial plane has reduced electron density as compared with the lone pair orbital in the axial plane.[49] Thus, the regions of the lowest electrostatic potential for the **TBP**^{e} structure of PF_4O^- are in accord with the direction of the lone pair orbital in the axial plane. We observed a similar trend for the dianionic cyclic oxyphosphorane **2a**[10] and for the related open-chain species.[50] For axially hydroxyl-substituted PF_4OH, the second-order perturbation energies of hyperconjugation do not reveal any significant difference between the **TBP**^{a} and **TS**$^a_{rot.}$ structures. This result is in accord with the fact that the axially substituted **TBP**^{a} structure of anionic PF_4O^- shows less directional electrostatic potential.

Comparison of Pseudorotation Processes for Neutral PF_4OH and Anionic PF_4O^-. Let us now consider the pseudorotation processes of neutral PF_4OH and

(47) McDowell, R. S.; Streitwieser, A. *J. Am. Chem. Soc.* **1985**, *107*, 5849−5855.
(48) Wang, P.; Zhang, Y.; Glaser, R.; Reed, A. E.; Schleyer, P. v. R.; Streitwieser, A. *J. Am. Chem. Soc.* **1991**, *113*, 53−64.
(49) The population of the p orbital in the equatorial plane was calculated to be 1.663, while the corresponding population in the axial plane was 1.792.
(50) Uchimaru, T.; Uebayasi, M.; Tanabe, K.; Taira, K. *FASEB J.* **1993**, *7*, 137−142.

anionic PF_4O^- species with the oxygen atom as the pivot. The barrier heights of these processes correspond to the energy difference between the trigonal bipyramidal structure and the square pyramidal structure (**TBP^e** and **TS$_{pr}$1** structures). The oxygen atom occupies the equatorial and the apical position, respectively, in these structures. The hydroxyl group has larger electronegativity than the oxy anion. Holmes's formulation[37] predicts, therefore, that anionic PF_4O^- should pseudorotate more readily than neutral PF_4OH. Holmes's formulation gives the estimations of 3.3 and 2.0 kcal/mol, respectively, for the pseudorotational barriers of PF_4OH and PF_4O^-.[51] The HF barrier height was calculated to be 9.9 kcal/mol for the pseudorotation of neutral PF_4OH. The corresponding barrier height for anionic PF_4O^- was 3.1 kcal/mol. Moreover, we carried out MP2 full geometry optimizations and then evaluated MP2 barrier heights.[52] The MP2 barrier heights were found to be 9.0 and 2.3 kcal/mol, respectively, for PF_4OH and PF_4O^-.

In accord with Holmes's prediction, the calculations suggested a lower barrier height for anionic PF_4O^- than for neutral PF_4OH. However, the HF and MP2 barrier heights for neutral PF_4OH were both significantly larger than the predicted value, while the agreement of the calculated barrier heights with the predicted value was much better for anionic PF_4O^-. The difference in electronegativities between hydroxyl group and oxy anion has been taken into account in Holmes's formulation. The deviation between the predicted and calculated values for neutral PF_4OH is understandable given the electrostatic interactions that are due to positively charged hydrogen. The anionic PF_4O^- shows directional electrostatic potential for the **TBP^e** structure, whereas the electrostatic potential for the square pyramidal (**TS$_{pr}$1**) structure is less negative and less directional (see Figure 9). Thus, the electrostatic stabilization is less important in the transition state (**TS$_{pr}$1**) than in the ground state (**TBP^e**). The hydrogen atom on the equatorial oxygen in the **TBP^e** structure of PF_4OH occupies the region with the lowest electrostatic potential. The positive charge on the hydrogen results in favorable electrostatic interaction and the additional lowering of the energy of the **TBP^e** structure for neutral PF_4OH.[53] The anionic PF_4O^- species does not involve this type of electrostatic interaction. The electrostatic stabilization due to the positive charge on the hydrogen of the P−OH bond in neutral PF_4OH results in the pseudorotational barrier being higher than predicted.[54]

Discussion

Recently, Beese and Steitz proposed that the exonuclease activity of the Klenow fragment of DNA polymerase involves two metal ions.[13] Such a double-metal ion mechanism has been postulated subsequently for several enzymatic RNA-cleavage reactions.[14−16,50] This mechanism postulates that metal cations are located between the nonbridging and attacking/departing oxygens in the trigonal bipyramidal intermediate/transition state. Taking the results of all our calculations together, we can extrapolate the effects of the coordination of metal ions in the double-metal ion mechanism.

The geometries of the transition states during cleavage/formation of the axial P−O bond for **2c** suggest a favorable electrostatic interaction between the axial oxygen and the hydrogen on the equatorial oxygen. The conformational preferences of the equatorial P−OH bond in **2c** and in PF_4OH can be rationalized in terms of the electrostatic interactions that are due to a positively charged hydrogen on the oxygen,[55] as well as the hyperconjugative interactions. The hydrogen of the P−OH bond in the equatorial position "prefers" the eclipsed positions relative to the axial ligands. The preferred location of the hydrogen is in accord with the regions where the corresponding anionic species has the lowest electrostatic potential. By contrast, the hydrogen in the equatorial plane significantly destabilizes the trigonal bipyramidal structure (**TS$_{rot}$1** and **TS$_{rot}$2** for **2c**, and **TS$^e_{rot}$** for PF_4OH). Meanwhile, the axially hydroxyl-substituted structure and the square pyramidal structure show less directional electrostatic potential. Correspondingly, the energies of these structures are less sensitive to the conformation of the P−OH bond than the energies of the equatorially substituted structures.

The higher pseudorotational barrier for PF_4OH, as compared with that for PF_4O^-, stems, at least in part, from the electrostatic stabilization due to the positively charged hydrogen of the P−OH bond. This observation suggests that the electrostatic effect of the cationic species on the pivot at oxygen acts to increase the barrier heights for pseudorotation. If cationic species are located and fixed in the regions between the nonbridging and attacking/departing oxygens, the trigonal bipyramidal intermediate/transition state should be stabilized for the in-line mechanism. Meanwhile, the cationic species in these regions act to discourage the positional exchange of ligands via pseudorotational processes. The coordination of metal ions in the double-ion mechanism should result in the electrostatic interaction that stabilizes exclusively the intermediate/transition state for the in-line mechanism. As a consequence of these effects, the cationic species at the active sites of enzymatic cleavage of RNA facilitate only the in-line attack and departure processes.

In the double-metal ion mechanism, divalent metal ions, such as magnesium(II) and zinc(II), are located in the catalytic active sites of the enzymes in question. Each enzyme may have a different organization of ligands for the metal cations in the active site and the detailed structures of metal ligands remain obscure. However, the net charges of the metal ions in the active sites are probably more positive than those of the hydrogens on the equatorial oxygens in **2c** and PF_4OH.[56] The electrostatic interactions would, thus, be larger in

(51) The electronegativity of the hydroxyl group and that of the oxy anion were assumed to be 3.7 and 2.5, respectively.[30,37]

(52) The MP2 absolute energies (au) and zero-point energies (not scaled: kcal/mol) of MP2 optimized geometries are as follows. For PF_4OH: −815.081 87, 18.13 (**TBP^e**); and −815.067 51, 17.25 (**TS$_{pr}$1**). For PF_4O^-: −814.581 77, 9.83 (**TBP^e**); and −814.578 13, 9.70 (**TS$_{pr}$1**).

(53) The **TBP^e** structure of neutral PF_4OH suggested a net charge of +0.54e for hydrogen on the equatorial oxygen.

(54) The protonation state of the pivot oxygen is also expected to affect the pseudorotation processes of cyclic species **2b** and **2c**. While neutral **2c** pseudorotates with the hydroxyl oxygen acting as the pivot, the oxy anion is the pivot for the pseudorotation of monoanionic **2b**. However, we were unable to give a clear interpretation regarding the pseudorotation processes of **2b** and **2c**. Since the pseudorotations for PF_4OH and anionic PF_4O^- give identical **TBP^e** structures at both ends, the energy profiles for pseudorotation processes of these species are symmetrical. By contrast, the end products for the pseudorotations of cyclic **2b** and **2c** are not the same and, thus, the energy profiles for pseudorotations of **2b** and **2c** are asymmetrical. As compared with neutral **2c**, anionic **2b** has a highly asymmetric profile, probably due to intramolecular electrostatic interaction between the oxy anion and the hydrogen of the P−OH bond in monoanionic **2b**. The calculated pseudorotation barrier heights were less than 7 kcal/mol for both **2b** and **2c** (see text).

(55) The positive charges of the hydrogen atoms on the equatorial oxygens in **2c** were found to be comparable to that of the hydrogen in PF_4OH. The stationary points of **2c** gave net charges between +0.54e and +0.62e for hydrogens on the equatorial oxygens.

the double-ion mechanism than we have calculated for our model systems.

In conclusion, the findings described in this paper provide a rationalization for metal coordination in the double-metal ion mechanism of ribozymes. The role of cationic species in the active sites for general ribonucleases is similarly understandable. The metal coordination should produce an electrostatic field that promotes the in-line attack and departure process and, concomitantly, prevents pseudorotations for the positional exchanges of ligands of pentacoordinate oxyphosphorane intermediate/transition state. Moreover, the metal cations located close to axial ligands are capable of enhancing nucleophilicity of the attacking oxygen and also of neutralizing the negative charges of the departing oxygen.[10,59] That is, positively charged metal cations stabilize oxyphosphorane structures through enhancement of the electronegativity of the axial ligands. These speculations also support the proposed double-metal ion mechanism for reactions catalyzed by ribozymes (Figure 10).[60]

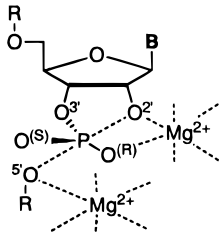

Figure 10. Proposed coordination of two magnesium ions at the catalytic active site of a hammerhead ribozyme.[60]

Acknowledgment. The services and computational time made available by Research Information Processing Center (RIPS) have been essential to this study and are gratefully acknowledged. We greatly appreciate our colleague Dr. Bruce W. Baldwin. Without his critical comments and advice, our discussion in this paper would undoubtedly have been less convincing.

JO951517+

(56) Glusker *et al.* examined the Cambridge Structural Database in an investigation of coordination states of metal cations in the crystal structures of organic molecules. Magnesium(II) ion complexes show a preference for a coordination number of six, whereas zinc(II) ion complexes show various coordination numbers, which are generally four, five, or six. The generalized second-order densities suggested net charges of +1.18e and around +1.4e for hydrated magnesium and zinc cations, respectively, with the preferred coordination numbers.[57,58]

(57) Bock, C. W.; Kaufman, A.; Glusker, J. P. *Inorg. Chem.* **1994**, *33*, 419−427.

(58) Bock, C. W.; Kaufman, A.; Glusker, J. P. *J. Am. Chem. Soc.* **1995**, *117*, 3754−3765.

(59) Uchimaru, T.; Tanabe, K.; Uebayasi, M.; Taira, K. *Chem. Express* **1992**, *7*, 501−504.

(60) Sawata, S.; Komiyama, M.; Taira, K. *J. Am. Chem. Soc.* **1995**, *117*, 2357−2358.